Received: 24 March 2020 | Revised: 14 May 2020 | Accepted: 27 May 2020

DOI: 10.1111/ijac.13570

ORIGINAL ARTICLE

International Journal of Applied Ceramic TECHNOLOGY

C/C-SiC component for metallic phase change materials

Veronika Stahl[1] | **Yuan Shi**[2] | **Werner Kraft**[1] | **Tim Lanz**[1] | **Peter Vetter**[1] | **Raouf Jemmali**[2] | **Fiona Kessel**[2] | **Dietmar Koch**[3]

[1]Institute of Vehicle Concepts, German Aerospace Center, Stuttgart, Germany

[2]Institute of Structures and Design, German Aerospace Center, Stuttgart, Germany

[3]Institute of Materials Resource Management, University of Augsburg, Augsburg, Germany

Correspondence
Yuan Shi, Institute of Structures and Design, German Aerospace Center, Pfaffenwaldring 38-40, 70569 Stuttgart, Germany.
Email: yuan.shi@dlr.de

Funding information
Technology Marketing of German Aerospace Center (DLR); German Aerospace Center

Abstract

Thanks to their high energy density and thermal conductivity, metallic Phase Change Materials (mPCM) have shown great potential to improve the performance of thermal energy storage systems. However, the commercial application of mPCM is still limited due to their corrosion behavior with conventional container materials. This work first addresses on a fundamental level, whether carbon-based composite-ceramics are suitable for corrosion critical components in a thermal storage system. The compatibility between the mPCM $AlSi_{12}$ and the Liquid Silicon Infiltration (LSI)-based carbon fiber reinforced silicon carbide (C/C-SiC) composite is then investigated via contact angle measurements, microstructure analysis, and mechanical testing after exposure. The results reveal that the C/C-SiC composite maintains its mechanical properties and microstructure after exposure in the strongly corrosive mPCM. Based on these results, efforts were made to design and manufacture a container out of C/C-SiC for the housing of mPCM in vehicle application. The stability of the component filled with mPCM was proven nondestructively via computer tomography (CT). Successful thermal input- and output as well as thermal storage ability were demonstrated using a system calorimeter under conditions similar to the application. The investigated C/C-SiC composite has significant application potential as a structural material for thermal energy storage systems with mPCM.

KEYWORDS

ceramic matrix composites (CMCs), corrosion, joints/joining, mechanical properties

1 | INTRODUCTION

Energy storage solutions are required because supply from renewable resources temporally and spatially mismatched to demand from consumers.[1-3] In general, the storage of thermal energy can be cheaper and more resource-conserving than storage of electrical energy[4] and is more reasonable in cases where thermal energy is finally needed by the user. A general requirement of thermal energy storage materials is a high energy density. This can be achieved through the use of latent energy systems, especially operated at high temperatures. A considerable advantage of metallic Phase Change Materials (mPCM) compared to molten salts and inorganic PCM is their high thermal conductivity.[5,6] This is especially apparent in applications where high thermal input and output is required. Battery electric vehicles (BEV) are such an application where rapid charging and discharging are vital. Thermal energy storage based on mPCM is a promising solution to the thermal management requirements of BEV.[7] A thermal storage system utilizing mPCM can supply the thermal energy demand of heating the passenger cabin without decreasing the electric vehicles range, which is the case for common solutions with electrical heaters.

However, the drawback is the high reactivity of mPCM especially in the liquid state with potential container materials.[8-12] Thus, there is a need to build a container for mPCM in vehicle application out of a novel compatible container

material. Due to their favorable mechanical properties at high temperature, corrosion resistance, and comparatively low density, Ceramic Matrix Composites (CMCs) have received considerable attention in aerospace and other applications in recent years.[13-15] Based on the results of previous studies for mechanical response and corrosion behavior,[16,17] carbon fiber reinforced silicon carbide (C/C-SiC) composite could be a promising candidate CMC for vehicle thermal storage applications due to its excellent corrosion resistance, low density, high damage resistance, and thermal shock resistance.

In this work, the compatibility between C/C-SiC and the mPCM $AlSi_{12}$ wt% (abbreviation: $AlSi_{12}$) is tested via contact angle measurements, exposure tests with subsequent mechanical three-point bending (3PB) testing and microstructural analysis as well as via liquid metal infiltration test. Furthermore, a C/C-SiC container, designed and manufactured according to boundary conditions of a BEV application scenario, is filled with mPCM via a pouring step and tested nondestructively via computer tomography (CT). The thermal storage ability and charging/discharging characteristics of the filled container component is characterized using a thermal energy storage system calorimeter under conditions similar to the BEV application.

2 | EXPERIMENTAL PROCEDURE

2.1 | Metallic phase change material

The mPCM selected was the eutectic binary alloy $AlSi_{12}$ wt%. ($AlSi_{12}$) This material was chosen primarily for its suitable melting temperature, high energy density, and high thermal conductivity. In Table 1 the most important properties of $AlSi_{12}$ are summarized. Commercially available casted $AlSi_{12}$ bars (technical grade) were used as raw materials (Supplier: Oetinger Aluminium NU GmbH, Grade: Al Si13Mg SK Block).

2.2 | C/C-SiC sample

In this work, C/C-SiC samples were manufactured via the Liquid Silicon Infiltration (LSI) process, which can be subdivided into three main process steps. In the first step, CFRP (Carbon Fiber Reinforced Polymers) preforms were manufactured via warm pressing ($T_{max} = 240°C$, $P_{max} = 5.8$ kPa), using prepregs based on phenolic resin precursor and a 2D carbon fiber fabric. In the subsequent carbonization stage, the green body was pyrolyzed at a temperature above 900°C under a nitrogen atmosphere and the polymer matrix was transformed to a carbon matrix. Finally, liquid silicon was infiltrated into the porous C/C structure (at $T_{max} > 1420°C$) by capillary forces and reacted with the carbon matrix to form silicon carbide. Due to the processing method, the final C/C-SiC was a dense multiphase material (density 1.80 g/cm^3; open porosity ~ 2%), characterized by load bearing carbon fiber bundles (~55 vol.%) embedded in a SiC matrix (~14 vol.%) with a small amount of residual Si (~3 vol.%) and C (~26 vol.%).

The fiber volume content (FVC) of the samples was calculated by considering the measurement of the initial weight of the fibers and the total volume of the finished component. That is:

$$\mathrm{FVC} = \frac{(W_F/\rho_F)}{V_C}100 = \frac{(W_F/\rho_F)}{(V_M + V_F)}100 \quad (1)$$

where W_F is the weight of the fibers, ρ_F is the density of the fibers, V_M is the volume of matrix, V_F is the volume of fibers, and V_C is the total volume of the finished sample.[18] The dry component was first weighed under normal atmospheric conditions, and then, weighed while submerged in water. Finally, it was weighed wet after being taken out of the water. Using the Archimedes principle, the following equation may be used to determine open porosity:

$$e' = \frac{W_{wet} - W_{wet}}{W_{dry} - W_{water}}100 \quad (2)$$

where W_{dry} is the weight of the sample under normal atmospheric conditions, W_{water} is the sample submerged in water, and W_{wet} is the sample after being taken out from water. The FVC and open porosity of the tested C/C-SiC plates were 57.0% and 2.3%, respectively.

2.3 | Methods

The compatibility between liquid mPCM and C/C-SiC plates was first analyzed with a contact angle measurement. The contact angles of mPCM-sample on the surface of C/C-SiC were measured with a DSAHT17-1 from Krüss GmbH in an argon atmosphere. In this test, solid mPCM-sample with a mass of about 44 mg was placed on a C/C-SiC substrate and the setup was heated to different

Melting temperature	Specific heat of fusion	Specific heat capacity	Thermal conductivity	Density
577°C	481 ± 30 J/g	0.88 ± 0.09 J/gK*	192 W/mK*	2.688 g/cm^3*

TABLE 1 Properties of $AlSi_{12}$ determined experimentally via dilatometry, differential scanning calorimetry, and laser flash analysis (* at 20°C)

temperatures. After investigating wetting behavior, an exposure test was performed. C/C-SiC samples were dipped into a bath of liquid mPCM at 700°C under ambient atmosphere and pressure for 4 hours. The samples were not completely covered by liquid mPCM, but the relevant section for subsequent mechanical testing was. The test was performed in a melting furnace which heats and melts the mPCM via indirect resistive heating and which controls the temperature via a pyrometer. After removal, the samples were cooled down to room temperature by natural convection. The setup is displayed in Figure 1.

It was of interest to determine whether the mechanical properties of C/C-SiC material changed after exposure to the liquid mPCM. The mechanical properties of the C/C-SiC material in an unexposed state and after exposure in the mPCM were investigated and evaluated through 3PB tests according to DIN EN 658-3 with a span-to thickness ratio L/t of 20.[19] The coupons for the 3PB test were water cut from the composite plate (approx. 80 mm * 80 mm with thickness of 2.3 mm) and the geometry of 3PB coupon is 10*2.3*50 mm^3 (width*thickness*length).

The longitudinal strains were measured with strain gauges on the tensile site of bending specimens. The experiments were performed at room temperature up to the failure of the sample by a universal testing machine (Zwick 1494) at a controlled cross head speed of 1 mm/min. The failure stress was calculated from the maximum load. For statistical confirmation, three samples of the composite in the unexposed state and after exposure were tested. Furthermore, the microstructure of C/C-SiC sample before and after molten mPCM exposure was evaluated by Scanning Electron Microscopy (SEM, Gemini ultra plus from Zeiss Group).

In order to determine whether the porous C/C-SiC withstand leakage of mPCM, a liquid metal penetration test was performed. For this test, a liquid mPCM column was positioned on a C/C-SiC plate with the help of a flanged pipe (see Figure 2). After pouring the mPCM into the flanged pipe, the setup was held at 600°C for 1 hour. The setup occasionally was shaken manually.

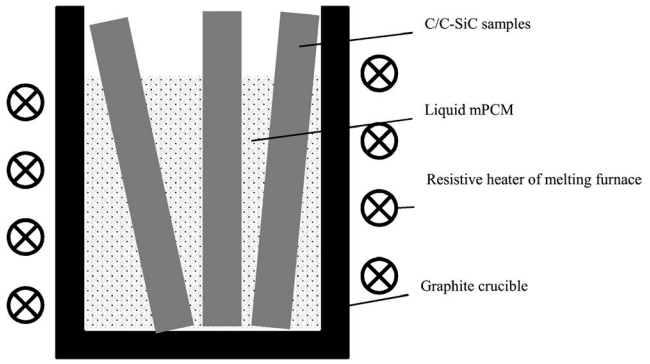

FIGURE 1 Setup of exposing C/C-SiC samples to liquid mPCM at 700°C for 4 hours

After concluding the fundamental investigation on material compatibility, the design of a container component out of C/C-SiC was approached. The application scenario provided the boundary conditions affecting the main design parameters. The single parts of the container were manufactured from resin pre-impregnated fabric (prepreg) or via the fabric winding technique. These parts were cured and pyrolyzed. For the lids, notches for the joining and holes for pouring and venting were machined through milling and grinding technique in the C/C state. Later, all parts were joined to a C/C preform with a joining paste. In the last process step, the resulting C/C container structure was siliconized. After a final machining step, mPCM was poured into the container component. The manufacturing process is described in more detail later in this article, as it depends on the identified boundary conditions and design. The quality and integrity of the container was monitored frequently via CT during the whole production process. The micro-focus computed tomography (μCT) scans were conducted using a high resolution μCT-System (v|tome|x L, GE Sensing & Inspection Technologies GmbH, Wunstorf) consisting of a micro-focus X-ray tube with a maximum accelerating voltage of 240 kV and a 16-bit flat panel detector (active area 2348 × 2348 pixels at 200 microns per pixel). The μCT scan parameters are summarized in Table 2. The acquired 2D X-ray images were reconstructed with a special reconstruction algorithm known as Filtered Back Projection, which is integrated in the reconstruction module datos|x of the CT system manufacturer. The μCT data were visualized and analyzed with the software package VGStudioMax 3.2 (Volume Graphics, Heidelberg).

Apart from CT scans, also internal pressure tests of the containers were performed to give some information about the quality of the joints and the mechanical stability. For the test, the clinched pouring nozzles were fused to be airtight and used as connection to the compressed air source. Soap suds were put on the components surface in order to optically detect the source of eventual bubbles, and thus, the location of defects as the pressure in the container was raised slowly. In order to test the components thermal energy storage ability under application conditions, a test setup for calorimetric analysis of metallic latent thermal energy storage systems was used. This method and the device are described in more detail in the previous work.[20]

3 | RESULTS AND DISCUSSION

3.1 | Material compatibility tests

3.1.1 | Contact angle measurements

The compatibility between liquid mPCM and C/C-SiC plates was first analyzed with a contact angle measurement. Measuring the contact angle between a liquid mPCM droplet

and a substrate sample gives information about the wetting behavior of the material combination. A contact angle larger than 90 ° is considered non-wetting and a contact angle smaller than 90° is considered wetting. If wetting is observed, it can be further categorized as either reactive or nonreactive wetting.[21]

First, at temperature of 700°C, 123 K above the mPCM melting temperature, a passivating alumina shell is present on the surface of aluminum alloys (Figure 3A). In the mobile application of interest, this shell can be stripped of by relative motion of the melt in the container due to vibration or driving induced sloshing. Then, in order to determine the wetting behavior in this worst case scenario, the alumina shell around the wetting sample needed to be removed. In this experiment the alumina shell was broken by increasing the test temperature to 1100°C. At this temperature, it could be observed that the solid alumina shell broke and the molten sample changed its shape to a droplet. However, the observed contact angle of 125° (Figure 3B) still could be affected by remaining parts of the broken alumina shell. Nevertheless, no tendency to neither reactive nor nonreactive wetting was observed. It was concluded that a non-wetting behavior would also be observed at lower temperatures when an alumina shell would be absent.

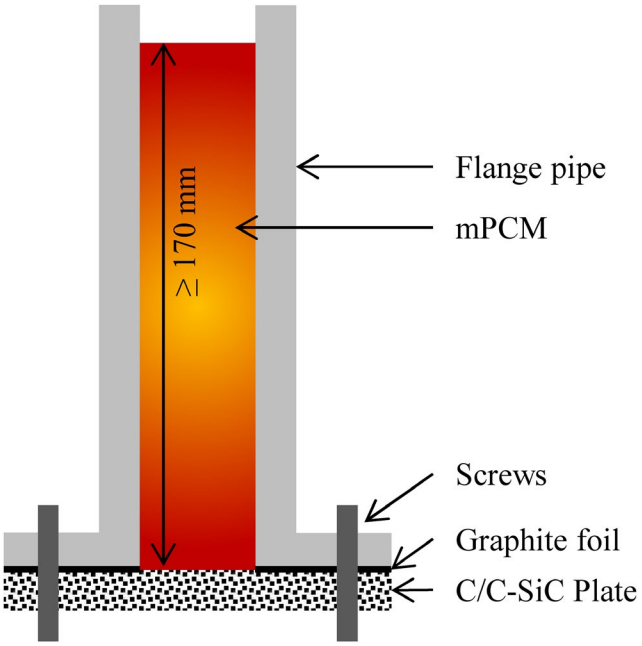

FIGURE 2 Liquid metal penetration test setup

3.1.2 | Exposure test

After investigating wetting behavior, an exposure test was performed. The stress-strain response in Figure 4 shows a quasi-ductile behavior for all the coupons before and after exposure. No significant influence of exposure in the molten mPCM on the bending properties of C/C-SiC materials could be determined. The measured 3PB-strength (σ_{3PB}), Young's modulus (E), and strain of failure (ε_{3PB}) are summarized in Table 3.

The sample before exposure shows the "block formation" (see Figure 5A), which is typical for C/C-SiC material [22]. That is, carbon fiber bundle forms block-like parts which are separated and encapsulated by Si and SiC veins (Figure 5A). Figure 5B shows the cross section of C/C-SiC sample after exposure in the molten mPCM for 4 h at 700°C. The sample was cleaned in an ultrasonic bath before image acquisition. In comparison with Figure 5A, the analysis of the exposed samples shows that the microstructure

Voxel size	Voltage	Current	Exposure time	Number of projections	Averaging/ Skip	Rotation
125 µm	220 kV	800 µA	500 ms	2400	3/1	360°

TABLE 2 Summary of CT scan parameters

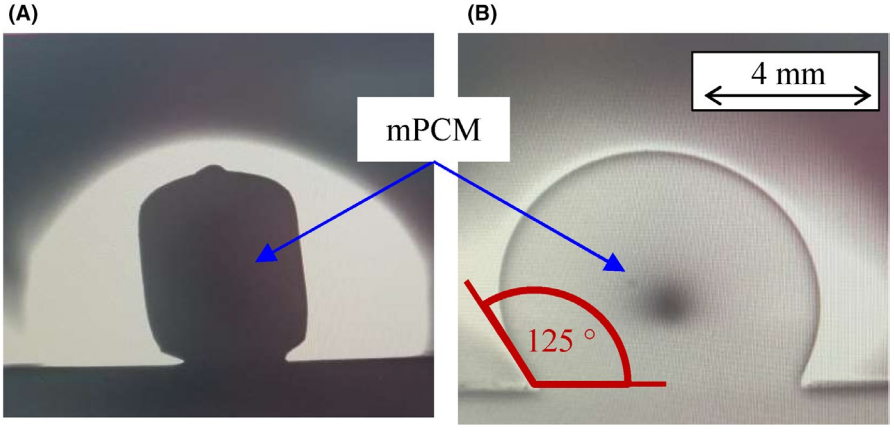

FIGURE 3 (A) Before and (B) after breaking the oxide layer around the mPCM sample at 1102°C, still non-wetting behavior on C/C-SiC substrate can be observed

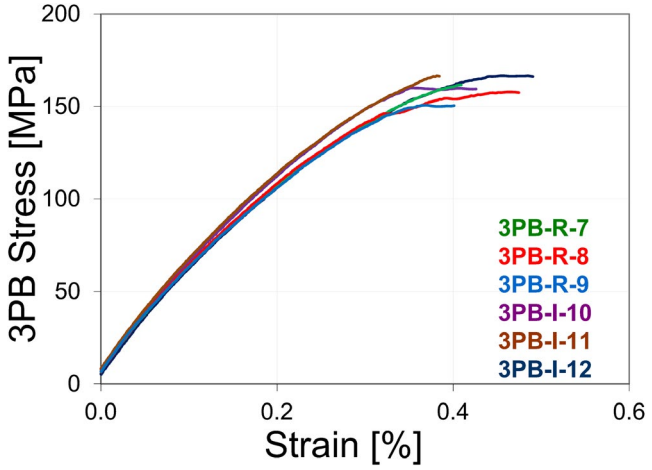

FIGURE 4 Stress-strain curves of 3PB tests for the coupons without exposure (3PB-R-7 to −9) and with exposure (3PB-I-10 to −12)

does not undergo microscopically observable changes after exposure (Figure 5B).

Based on the results of contact angle measurements and exposure test, the material combination between $AlSi_{12}$ and C/C-SiC shows non-wetting behavior up to at least 1102°C and mechanical properties as well as microstructure did not change significantly after exposure. For this reason, additional coating for corrosion resistance is not necessary.

3.1.3 | Liquid metal penetration test

Besides compatibility, another central requirement to materials containing liquid mPCM is that no leakage occurs. Due to the open porosity of C/C-SiC, liquid is able to permeate if pore radius r is large enough. A relation between this radius, pressure to permeate P, surface tension of the liquid γ_{LV}, and wetting angle θ is given by Young-Laplace equation:

$$P = \frac{2 \cdot \gamma_{LV} \cdot \cos(\theta)}{r} \tag{3}$$

For the case that only gravitation promotes infiltration, P equals the hydrostatic pressure P_H.

In order to determine whether the C/C-SiC pores are small enough to withstand the hydrostatic pressure arising from the mPCM mass, a liquid metal penetration test was performed. The height h of liquid mPCM column was larger than 170 mm, which corresponds to a hydrostatic pressure P_H of over 0.04 bars according to Equation 4. The density ρ of $AlSi_{12}$ at 600°C is 2.48 g/cm^3 and g is the gravity acceleration of 9.81 m/s^2.

$$P_H = h \cdot \rho \cdot g \tag{4}$$

After the test no liquid metal penetration into the pores could be observed and no leakage occurred. Thus, in several tests the material compatibility of $AlSi_{12}$ and C/C-SiC could be shown in terms of wetting behavior, change of mechanical properties, change of microstructure and leakage.

TABLE 3 Summary of results from 3PB testing

Exposure in mPCM	σ_{3PB} [MPa]	E [GPa]	ε_{3PB} [%]
No	156.7 ± 5.6	64.2 ± 0.9	0.41 ± 0.05
Yes	164.4 ± 3.8	65.2 ± 1.9	0.40 ± 0.05

3.1.4 | Possible reactivity between Al-Si-alloys with compositions of C/C-SiC

To the best of the authors' knowledge, up to now there is no specific investigation about the reactivity between Al-Si-alloys with C/C-SiC in literature. However, several articles have discussed the possible reactivity of molten aluminum alloys with the components of the investigated C/C-SiC material, which are in particular carbon (C), silicon carbide (SiC), and a small amount of residual silicon (Si).

First, in the binary system of aluminum-carbon, the aluminum carbide Al_4C_3 is the only intermediate compound as well as the thermodynamically favored compound of reaction (1) above the melting point of aluminum.[23]

$$4\,Al + 3\,C = Al4C3 \tag{5}$$

Then, in regard to SiC and as SiC is considered as solid matter, reaction Equation (2) is relevant for the whole system. For molten aluminum-silicon alloys, Schwabe *et al* additionally proposed reaction (3. When combining Equations (2) and (3) there is an equilibrium between SiC, Al_4C_3, and a liquid mixture. The equilibrium composition of the liquid Al-Si-mixture largely depends on small changes in Gibbs enthalpy, the constituent activities and the different temperatures.[23-27]

$$3\,SiC\,(s) + 4\,Al\,(l) = Al_4C_3(s) + 3\,Si\,(l) \tag{6}$$

$$Si + xAl = \{Si - Al_x\} \tag{7}$$

Furthermore, Yan and Fan additionally found that the microstructure of the product phase is strongly depending on the polarity and orientation of the substrate crystal, which can influence the severity of damage to the substrate surface.[23] Free Si in the microstructure can have additional effects like acting as diffusion pathways, and thus, enhancing corrosion even at grain boundaries.[27,28] Although stable carbides do exist in the

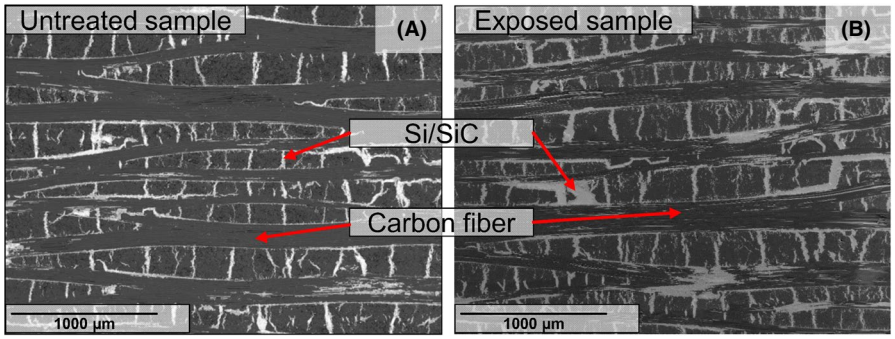

FIGURE 5 SEM images of C/C-SiC samples: (A) without exposure, and (B) after exposure

tested temperature range of this current work, several authors report that no carbide formation was observed after cycling or compatibility tests around 650°C.[29,30] Rodríguez-Guerrero *et al* observed evidence for Al_4C_3 formation like changed wetting behavior only at much higher temperatures.[31] It is well known that molten aluminum alloys are covered by a thin passivating layer of Al_2O_3 when exposed to air, which could inhibit reactivity with other solids.[23] However, Rawson *et al* discussed that the integrity of this oxide layer could be influenced under operation due to thermal cycling and shear stresses.[30]

In conclusion, potential reaction products between Al-Si mPCM and C/C-SiC are SiC and Al_4C_3. Reaction processes can be hindered by a passivating oxide layer on the molten alloy. Reaction processes are expected to depend on a large variety of influencing parameters, for example, temperature, silicon amount in the molten alloy, microstructure, crystal orientation, local deviations of Gibbs enthalpy, convection, diffusion pathways, integrity of passivating layers, and therefore, stresses due to cycling or shear, etc However, it should be noticed that one of the main scopes of this paper is to show, how a C/C-SiC component could be designed and produced as a container for the housing of mPCM in vehicle application. In this study, the first short-term tests about compatibility were performed and evaluated, indeed they cover only little time frames and not all influences of operation, therefore, it is strongly recommended to intensify the further studies on compatibility in future works.

3.2 | Container development

3.2.1 | Design

After concluding the fundamental investigation on material compatibility, the design of a container component out of C/C-SiC was approached. The container was to be built as simple and cost-efficient as possible. The application scenario provided the boundary conditions affecting the main design parameters. The process of defining design parameters is shown in Figure 6.

The cylindrical shape of the component resulted from the assumption of using a cylindrical heat extraction system. Such a cylindrical heat extraction system was proposed earlier[32]. The thermal output of 5 kW, defined by the application scenario, resulted in a required heat exchange area of 236 cm^2 which directly led to the length and radius of the inner cylinder. The central heat extraction system was surrounded by mPCM. The amount of material was defined by the heat capacity required by the application scenario, to 4.2 kg $AlSi_{12}$. The outer dimension was completed with an outer cylinder, while the top and bottom were closed with two lids. Due to different thermal expansion coefficients of mPCM and C/C-SiC and due to directional solidification, a mechanical force on the inner container cylinder was expected to arise during operation. Therefore, the wall thickness of the inner C/C-SiC cylinder was chosen to be able to resist this force while still being thin enough to not hamper heat transfer significantly. Based on experience in assembling C/C-SiC cylinders and through validation by thermal transient FEM-analysis with ANSYS, a final wall thickness of 3 mm was defined. Pouring holes and joints between the four single components completed the final design of the C/C-SiC container.

3.2.2 | Manufacture

At first, preforms for the top and bottom lids were manufactured separately using resin pre-impregnated fabric (prepreg) based on a phenolic resin precursor and a 2D carbon fiber fabric (Toho Tenax HTA40, 3K, twill weave, 245 g/m^2). The contour of the inner cylinder was produced using the fabric winding technique with same prepreg as for both lids. The fiber orientation of the inner cylinder was 0/90° and the inner diameter was 50 mm, 150 mm in length, and 3 mm thickness. The fiber preform of the outer cylinder was fabricated using a three axis filament winding machine by Waltritsch & Wachter. The carbon fiber tow was impregnated with phenolic resin precursor immediately before being wound on the mandrel. The fiber orientation of the outer cylinder was ± 15° and the inner diameter was 140 mm, with a length of 150 mm and thickness of 3 mm. The wet preforms of both lids, inner and outer cylinder were then cured separately

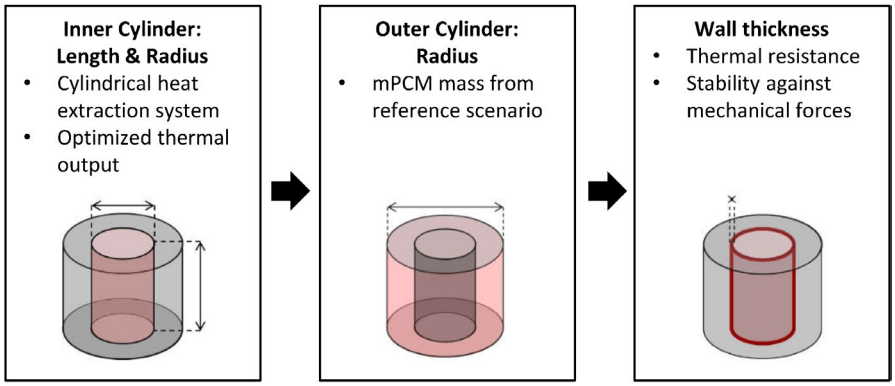

FIGURE 6 Process of defining design parameters of the container component

at approx. 200°C for 6 hours in an autoclave, producing a carbon-fiber reinforced polymer (CFRP) green body. For the inner and outer cylinder, no outer molds were used for additional consolidation to provide a simple and efficient curing process. The mandrels were removed after cooling to room temperature. The CFRP preforms were subsequently pyrolyzed at $T_{max} = 1650°C$ in a N_2 atmosphere at ambient pressure. Thereby the polymer matrix was transformed to a C matrix. The volume shrinkage of the matrix-induced internal stresses, leading to micro cracks and a 3D network of micro channels formed in the porous C/C composite. To avoid any contour deformation and ovalization due to shrinkage during pyrolysis, the inner contour of both cylinders were supported with graphite cores with the same shape and size as the mandrel. For both lids, notches for the joining and holes for pouring and venting were machined through milling and grinding technique in the C/C state. Later, the lid structures and the both cylinders were joined to a C/C preform with a joining paste based on the phenolic resin and a defined content of carbon powder. In the last process step, after joining the lids and cylinders, the resulting C/C container structure was siliconized at a temperature higher than 1420°C in vacuum. It should be noticed that during heating, the joining paste was pyrolyzed and transformed to a porous C material first, then reacted with Si granulate leading to a permanent join for the C/C-SiC structure.

In the application concept heat input as well as heat output occur over the inner cylinder. This process was to be simulated with a test bench where the heat transfer system would be implemented as a copper cylinder located at the center of the storage component. To achieve adequate thermal transport a good thermal contact between the inner C/C-SiC cylinder and copper cylinder was essential. Thermal contact depends on the surface structure as well as on the dimensions of both parts. Copper and C/C-SiC have different coefficients of thermal expansion, thus ensuring contact through dimension changes for different states of charge of the storage was necessary. Additionally, directional solidification and thermal expansion mismatch between the mPCM, C/C-SiC, and copper can lead to compression or elongation of the inner C/C-SiC cylinder during cooling and heating. The inner diameter of the inner C/C-SiC cylinder needed to be adjusted very precisely in order to ensure good thermal contact while avoiding high stresses which could have led to failure. In a final machining step the inner diameter of the component was adjusted mechanically via grinding. For filling the component, two nozzles were riveted in the designated holes. The nozzles acted as a vent, as a connection for a pouring cone and as were used to close the component. The final stage of manufacture involved pouring 4.2 kg of mPCM into the container component. The container component was preheated to 500°C and the inductively melted mPCM was poured through one pouring hole using a cone while the other pouring aperture acted as a vent hole. The manufacturing process, final machining, and pouring of the mPCM into the C/C-SiC container structure are shown in Figure 7.

3.2.3 | Application test

CT and pressure test

The quality and integrity of the container was monitored frequently via CT during the whole production process. The analysis occurred for the empty container as well as for the container filled with mPCM. The CT-results of the manufactured C/C-SiC container is shown in Figure 8A. Apart from CT scans, also internal pressure tests of the containers were performed. C/C-SiC is not completely airtight as it has a small amount of open porosity. However, gas may permeate through the container wall if pressurized. Thus, an internal pressure test on the empty component with compressed air can give some information about the quality of the joints and the mechanical stability.

At an internal gas pressure of one bar, though no gap between the joining interfaces of lid and cylinder can be found, a crack in the outer cylinder near the joining area was observed (Figure 8B). As the mechanical load at this internal pressure was several magnitudes lower than what the materials properties allow, it was deduced that the failure already existed before the pressure test was performed. It should be noted that, though no visible cracks from the CT-results before internal pressure tests can be observed in Figure 8A, which can

be explained that due to the limitation of the resolution of µCT, small cracks are not detectable. However, during the internal gas pressure test the size of existing cracks could be considerably increased, which were detectable after the test by means of the same µCT equipment. It is reasonable that this failure could have resulted from high manufacturing process temperatures. During LSI when producing C/C-SiC the process temperature can rise over 1420°C. The coefficient of thermal expansion in C/C-SiC is highly anisotropic. Where pieces are bonded with dissimilar orientation, a considerable mismatch in expansion coefficient may occur across the connection. This may have led to the fracture observed after the very high temperature siliconizing process. Hence, this process is the most critical step in manufacturing a C/C-SiC container component.

A further CT scan of the sample was performed after pouring the mPCM. It revealed delamination at the inner cylinder. Figure 9 shows a section of the filled component from top view where the failure is marked. Due to directional cooling after pouring and further contraction of the mPCM in solid state toward the inner cylinder, a load on the C/C-SiC component arose, which led to material failure. The delamination occurred only at the surface so that further component tests could be performed.

System calorimeter

In order to test the components thermal energy storage ability under application conditions, a test setup for calorimetric analysis of metallic latent thermal energy storage systems was used.[20] The setup (Figure 10) was equipped with an electrical heating unit in order to charge the storage component. The stored thermal energy could be determined through an energy balance considering electrical heat input, heat stored in the setup components, heat output by convection to a fluid, and heat loss to the surroundings.

Heat loss to the surroundings was determined as a calibration step in which the heat loss was correlated to the setups surface temperature during a heating process. In the

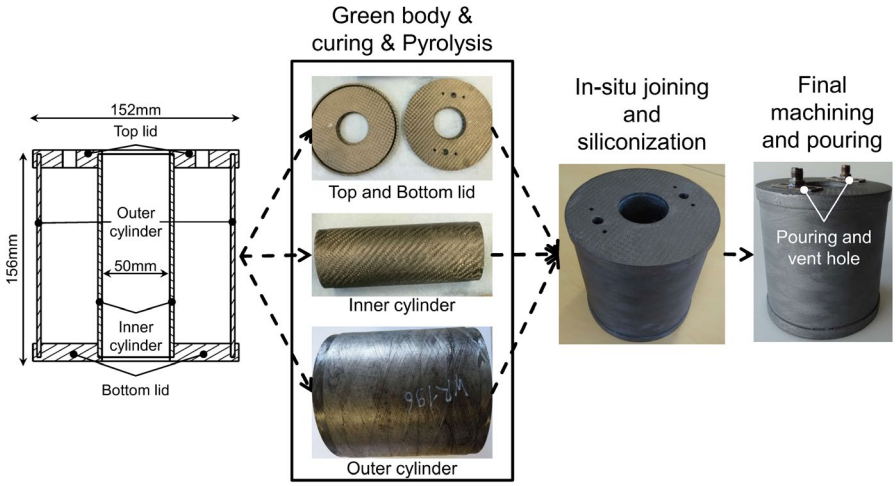

FIGURE 7 Scheme of manufacturing process, final machining, and poring of C/C-SiC container Structure

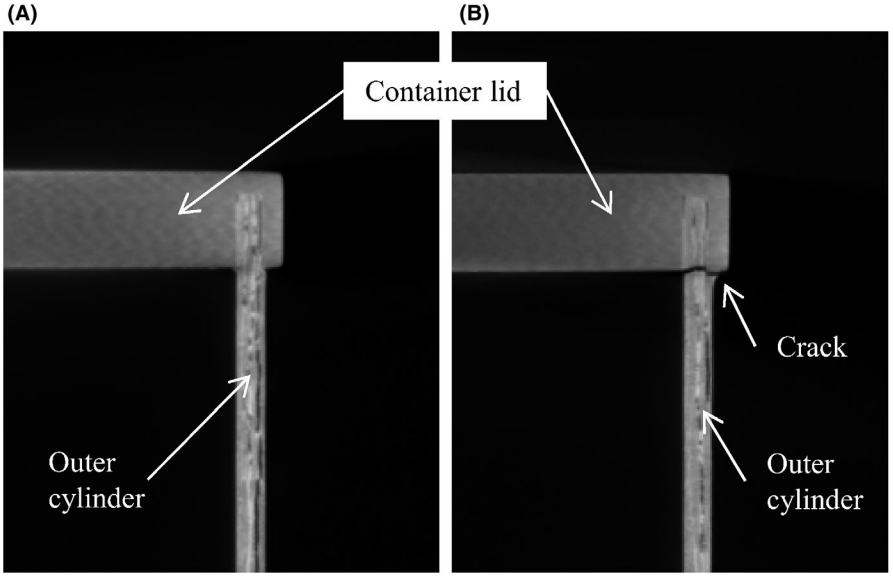

FIGURE 8 (A) CT-results of container before internal pressure test; (B) CT-results of container after internal pressure test and crack in the outer cylinder revealed by internal pressure test resulting from manufacturing process

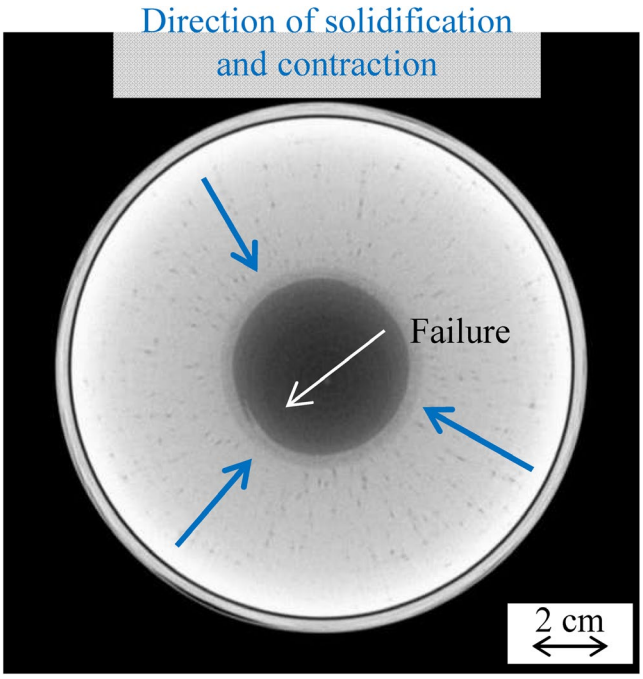

FIGURE 9 Delamination at the inner cylinder after pouring process resulting from mPCM solidification and contraction direction

subsequent cooling process heat was actively extracted by a working fluid passing through the components inner cylinder. The heat output to the working fluid was determined by measuring the fluids inlet and outlet temperatures as well as its mass flow rate. The resulting temperature as a function of time measured in the mPCM is shown in Figure 11. The test was performed for sample temperatures up to 300°C as the structural integrity of inner cylinder was not anymore given after the former tests. As the leakage of liquid mPCM could not be ensured, the calorimeter test was limited to a temperature in which $AlSi_{12}$ remains solid.

In the calibration phase different temperatures were approached and held with the aim to reach steady state. In steady state conditions heat loss to the surroundings equals the measurable power of the electrical heater. The time necessary to reach steady state depends on the thermal contact of the heater to the sample component and of the quality of the temperature controller settings. In Figure 11, it is shown that even after long equilibration times of up to 1 hour, steady state could often not be adequately reached. In the future, further focus needs to be put on improving thermal contact and measuring procedures for this sample. As a consequence, the observed behavior may induce large deviations of measured thermophysical properties from real values. Additionally, poor thermal contact and the use of air as a working fluid leads to a maximum heat output of only 1.8 kW.

By balancing all determined heat contributions, the thermal energy stored in the sample component as a function of temperature was determined and is displayed in Figure 12. In the component including mPCM storage material as well as C/C-SiC container material 1500 kJ thermal energy could be stored at 300°C. From the slope of stored thermal energy over temperature the heat capacity could be determined. A slightly increasing heat capacity with increasing temperature was observed. The specific heat capacity was obtained by referring to the mass of the filled component, 5.6 kg. The samples average specific heat capacity between room temperature and 300°C was found to be 1004 J/kg•K. The expected specific heat capacity calculated from mass fractions of mPCM and C/C-SiC container as well as from c_p values of

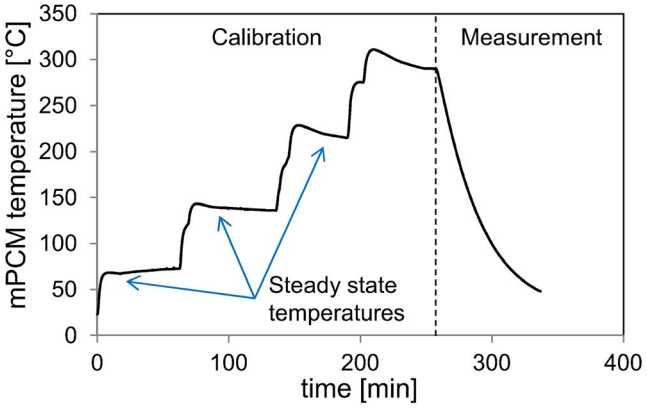

FIGURE 11 mPCM temperature over time during test of the filled C/C-SiC component in the system calorimeter

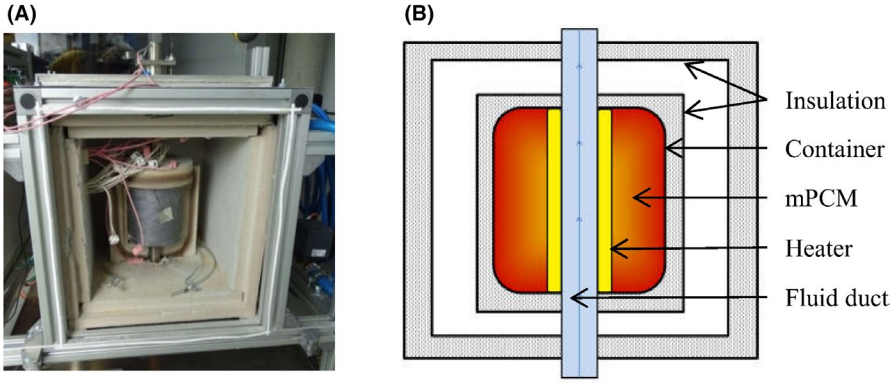

FIGURE 10 Photograph (A) and Scheme (B) of the system calorimeter used to characterize latent thermal energy storage components

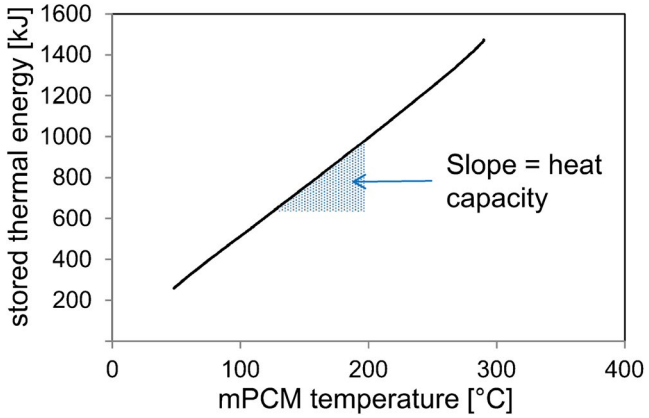

FIGURE 12 Thermal energy stored in the mPCM filled C/C-SiC container component as a function of temperature

each (see Table 1 and [22]) is 882 J/kg K. The overestimation of stored energy by the measuring method results from underestimating heat losses. This demonstrates the need for optimizing the system calorimetry method to this sample system and reduction of the thermal contact resistance between sample and the central heat transfer copper cylinder. However, it was possible to demonstrate the storage of thermal energy in the designed and manufactured storage component and the operability of the combination of C/C-SiC and mPCM as storage component was proven.

4 | CONCLUSIONS

Due to its excellent corrosion resistance C/C-SiC was expected to be a suitable solution for structural components in contact with $AlSi_{12}$ as an example for liquid mPCM. In several tests the material compatibility between $AlSi_{12}$ and C/C-SiC for short exposure durations was observed. The material combination shows non-wetting behavior up to at least 1102°C and mechanical properties as well as microstructure did not change significantly after exposure. As the material compatibility was proven, a C/C-SiC container was designed according to the requirements of a vehicle application. This functional model was manufactured and tested successfully up to 300°C. Input, output, and storage of thermal energy have successfully been demonstrated under conditions similar to the application in a system calorimeter. In future experiments, boundary conditions closer to those expected in the application should be achieved, these include higher temperatures, improving the heat output from 1.8 kW to the intended 5 kW, longer durations and thermal cycling.

Although the functionality to store thermal energy of the component could be shown, also failure of the component occurred resulting from manufacturing process and pouring process. Further research is planned to optimize fiber orientation of single component parts, which already indicates high potential to optimize functionality of the C/C-SiC component in this application.

Through C/C-SiC as a high cost material is crucial for commercialization in automotive applications, the key for an economical manufacturing is automatization and high production volumes. Examples like the commercialization of the C/C-SiC brake disc show that this material can be very successfully transferred to industry. With further adaptations in storage design and thermal transfer system the proposed thermal energy storage system could be of great energetic as well as economic advantages.

ACKNOWLEDGMENTS

This research is funded by Technology Marketing of German Aerospace Center (DLR). The authors would like to thank Matthias Scheiffele, Felix Vogel, Marco Alexander Smolej, and Daniel Cepli at the DLR-Institute of Structures and Design for their technical support. A sincere thanks to Anthony Rawson for his diligent proof reading.

ORCID

Yuan Shi https://orcid.org/0000-0002-4210-9069
Dietmar Koch https://orcid.org/0000-0003-4504-8721

REFERENCES

1. Dincer I, Rosen MA. Thermal energy storage: Systems and applications, 2nd edn. England: Wiley; 2010.
2. Abrell J, Rausch S, Streitberger C. Buffering volatility: Storage investments and technology-specific renewable energy support. Energy Econ. 2019;84(1):104463.
3. Azzuni A, Breyer C. Energy security and energy storage technologies. Energy Procedia. 2018;155:237–58.
4. Thess A, Trieb F, Wörner A, Zunft S. Herausforderung Wärmespeicher. Physik J. 2015;14(2):33–9.
5. Khare S, Dell'Amico M, Knight C, McGarry S. Selection of materials for high temperature latent heat energy storage. Sol. Energy Mater. Sol. Cells. 2012;107:20–7.
6. Kotze JP, von Backstrom TW, Erens PJ. High temperature thermal energy storage utilizing metallic phase change materials and metallic heat transfer fluids. J. Sol. Energy Eng. 2013;135(3):035001
7. Kraft W,Altstedde MK. Use of metallic Phase Change Materials (mPCM) for heat storage in Electric- and Hybrid Vehicles. 6th Hybrid and Electric Vehicles Conference (HEVC 2016), London. 2016:1–6. doi: 10.1049/cp.2016.0974.
8. Fernández AI, Barreneche C, Belusko M, Segarra M, Bruno F, Cabeza LF. Considerations for the use of metal alloys as phase change materials for high temperature applications. Sol. Energy Mater. Sol. Cells. 2017;171:275–81.
9. Andraka CE, Kruizenga AM, Hernandez-Sanchez BA, Coker EN. Metallic phase change material thermal storage for dish stirling. Energy Procedia. 2015;69:726–36.
10. Polkowski W, Sobczak N, Polkowska A, Bruzda G, Kudyba A, Giuranno D. Silicon as a phase change material: performance of h-bn ceramic during multi-cycle melting/solidification of silicon. JOM. 2019;71(4):1492–8.

11. Royo P, Acevedo L, Ferreira VJ, García-Armingol T, López-Sabirón AM, Ferreira G. High-temperature PCM-based thermal energy storage for industrial furnaces installed in energy-intensive industries. Energy. 2019;173:1030–40.
12. Xu H, Sadiki N, Magro FD, Py X, Mancaux J-M, Romagnoli A. Compatibility tests between molten Aluminium alloys and recycled ceramics from inorganic industrial wastes. Energy Procedia. 2017;142:3689–96.
13. Christin F. CMC Materials for space and aeronautical applications. Ceramic Matrix Composites: Wiley-VCH Verlag GmbH & Co. KGaA; 2008. p. 327–51.
14. Kohyama A. CMC for nuclear applications. Ceramic Matrix Composites: Wiley-VCH Verlag GmbH & Co. KGaA; 2008. p. 353–84.
15. Behrendt T, Hackemann S, Mechnich P, Shi Y, Hönig S, Hofmann S, et al. Development and test of oxide/oxide cmc combustor liner demonstrators for aero engines. J. Eng. Gas Turbines Power. 2017;139(3):031507. 10.1115/1.4034515
16. Li Y, Xiao P, Shi Y, Almeida RSM, Zhou W, Li Z, et al. Mechanical behavior of LSI based C/C-SiC composites subjected to flexural loadings. Compos. Part A - Appl. S. 2017;95:315–24.
17. Ding W, Shi Y, Kessel F, Koch D, Bauer T. Characterization of corrosion resistance of C/C–SiC composite in molten chloride mixture MgCl2/NaCl/KCl at 700 °C. npj Mater. Degrad. 2019;42(3):1–9.
18. DIN EN. (1389) Advanced technical ceramics - Ceramic composites - Physical properties - Determination of density and apparent porosity. 2004.
19. DIN EN, 658–3. Advanced technical ceramics - Mechanical properties of ceramic composites at room temperature - Part 3: Determination of flexural strength. 2003.
20. Jilg V, Kraft W, Lanz T, Vetter P, Feder F. eds. Methods and setup for calorimetric analysis of metallic latent thermal energy storage systems. Die 23 Kalorimetrietage; 2019; Braunschweig.
21. Eustathopoulos N. Dynamics of wetting in reactive metal/ ceramic systems. Acta Mater. 1998;46(7):2319–27.
22. Krenkel W. Development of a cost efficient process for the manufacture of CMC components. Doctoral Thesis, University of Stuttgart. 2000.
23. Yan M, Fan Z. Review Durability of materials in molten aluminum alloys. J. Mater. S. 2001;36(2):285–95.
24. Calderon NR, Voytovych R, Narciso J, Eustathopoulos N. Pressureless infiltration versus wetting in AlSi/graphite system. J. Mater. S. 2010;45(16):4345–50.
25. Calderon NR, Voytovych R, Narciso J, Eustathopoulos N. Wetting dynamics versus interfacial reactivity of AlSi alloys on carbon. J. Mater. S. 2009;45(8):2150–6.
26. Fukahori R, Nomura T, Zhu C, Sheng N, Okinaka N, Akiyama T. Thermal analysis of Al–Si alloys as high-temperature phase-change material and their corrosion properties with ceramic materials. Appl. Energy. 2016;163:1–8.
27. Schwabe U, Wolff LR, van Loo FJJ, Ziegler G. Corrosion of technical ceramics by molten aluminium. J. Eur. Ceram. Soc. 1992;9(6):407–15.
28. Mouradoff L, Tristant P, Desmaison J, Labbe JC, Desmaison-Brut M, Rezakhanlou R. Interaction between Liquid Aluminium and Non-Oxide Ceramics (AlN, Si3N4, SiC). Key Eng. Mater. 1995;113:177–88.
29. Reed S, Sugo H, Kisi E, Richardson P. Extended thermal cycling of miscibility gap alloy high temperature thermal storage materials. Sol. Energy. 2019;185:333–40.
30. Rawson AJ, Gläsel T, Nowak B, Boon D, Stahl V, Kargl F, et al. The compatibility of metallic thermal storage materials and housing materials: A computational survey and accelerated reaction experiments. In: Chen X, Zhong Y, Zhang L, Howarter JA, Baba AA, Wang C, eds. Energy technology 2020: Recycling. Carbon Dioxide Management, and Other Technologies: Springer International Publishing; 2020. p. 15–29.
31. Rodríguez-Guerrero A, Sánchez SA, Narciso J, Louis E, Rodríguez-Reinoso F. Rodríguez-Reinoso F. Pressure infiltration of Al–12wt.% Si–X (X=Cu, Ti, Mg) alloys into graphite particle preforms. Acta Mater. 2006;54(7):1821–31.
32. Lanz T, Jilg V, Kraft W, Vetter P, Volk BS. Experimental Evaluation of a Heat Transport System for a High-Temperature Storage Unit. Proceedings of 5th World Congress on Mechanical, Chemical, and Material Engineering (MCM'19); 2019; Lisbon, Portugal. DOI: 10.11159/htff19.161.

How to cite this article: Stahl V, Shi Y, Kraft W, et al. C/C-SiC component for metallic phase change materials. *Int J Appl Ceram Technol*. 2020;00:1–11. https://doi.org/10.1111/ijac.13570